Appl. Phys. A (2017) 123:374
DOI 10.1007/s00339-017-1003-5

Applied Physics A
Materials Science & Processing

A study about the influence of single-scale and dual-scale structures on surface wettability

Hao Li[1] · Sirong Yu[1] · Wenxian Xie[2] · Xiangxiang Han[1] · Xinhui Wang[2]

Received: 16 February 2017 / Accepted: 25 April 2017 / Published online: 26 April 2017

Abstract Surface morphology is known as the key factor to obtain lyophobic surface. This paper illustrates two superhydrophobic surfaces with different surface morphologies including single-scale nanorod structure and dual-scale flower-like structure. We compared contact angles of many liquids and dynamic behavior of water droplet impinging on the nanorod structured surface to those of on the flower-like structured surface. It was found that both the single-scale nanorod structure and the dual-scale flower-like structure can achieve superhydrophobicity. However, the dual-scale flower-like structure is superior to the single-scale nanorod structure in terms of repelling the droplet with low surface tension. In addition, we investigated stability and corrosion resistance of these two superhydrophobic surfaces, showing that both the single-scale nanorod and the dual-scale flower-like structured superhydrophobic surfaces had excellent long-term stability and thermal stability. Nevertheless, the dual-scale flower-like structured superhydrophobic surface was more stable under outside vibration and had better corrosion resistance than the single-scale nanorod structured superhydrophobic surface.

Electronic supplementary material The online version of this article (doi:10.1007/s00339-017-1003-5) contains supplementary material, which is available to authorized users.

✉ Sirong Yu
yusrchina@163.com

[1] College of Mechanical and Electronic Engineering, China University of Petroleum (East China), Qingdao 266580, People's Republic of China

[2] Shengli Oil Production Plant, Shengli Oilfield Company, SINOPEC, Dongying 257051, People's Republic of China

1 Introduction

Superhydrophobic surface has attract great attention due to many functions such as self-cleaning [1, 2], anticorrosion [3, 4], anti-icing [5] and anti-bacteria [6]. It has been well accepted that the combined effect of surface morphology and low surface energy contributes to the superhydrophobicity [7]. Inspired by the surface morphology of louts leaf [8, 9], researchers have successfully fabricate many superhydrophobic surfaces with hierarchical structures using various methods [10–13]. In addition, some superhydrophobic surfaces have single-scale structures. Shi et al. [14] fabricated single-scale nanorod superhydrophobic surface with water contact angle of 153.67° and the sliding angle of 4°. Lee et al. [15] prepared single-scale sharper pillar structured superhydrophobic surface by electrodeposition of nickel and Varanasi et al. [16] also reported single-scale pillar structured superhydrophobic surface.

In actual production, it also needs the superhydrophobic surface has oleophobicity or even superoleophobicity, repelling a variety of droplets. According to theoretical analysis, Patankar [17] has reported the result that both dual-scale roughness structure and slender pillars can contribute to amplifying apparent contact angle. Many superamphiphobic (both superhydrophobic and superoleophobic) surfaces have been successfully fabricated, and most of these superamphiphobic surfaces had hierarchical structures. The re-entrant structure plays a key role in achieving superamphiphobic for a wide variety of liquids [18–21]. For example, a hierarchical step-like microstructure with nanopores was fabricated on an Al surface through facile chemical etching and anodization, and this surface was conferred superamphiphobic after fluorination [22]. Marmur et al. reported the superamphiphobic nanocellulose aerogels, consisting of fibrillar networks and

aggregates with structures at different length scales [23]. Chen et al. fabricated a flower-like superamphiphobic surface by solvothermal process and self-assembly functionalization [24]. Jiang et al. prepared raspberry-like structured superamphiphobic coating [25] and Lee et al. fabricated superamphiphobic surface with mushroom-like micropillar arrays [26]. However, to the best of our knowledge, there was few article reported the superamphiphobic surface with single-scale structure. Jiang et al. fabricated a superamphiphobic surface with aligned carbon nanotube [27], repelling rapeseed oil with surface tension of ~35.7 mN/m [28].

In this paper, we investigated the effect of single-scale and dual-scale structures on surface wettability by comparing the ability of nanorod and flower-like structured superhydrophobic surfaces repelling to various droplets (water, glycerol, different ethanol concentration in water, and crude oil) and the dynamic behavior of water droplet on these two superhydrophobic surfaces. In addition, we investigated long-term stability, thermal stability, the stability of repelling outside vibration, and the corrosion resistance of these two superhydrophobic surfaces.

2 Experimental section

2.1 Materials

X90 pipeline steel was obtained from TGRC of China and cut into the size of 20 mm × 50 mm × 3 mm, and copper (purity of 99.9 wt%) and zinc (purity of 99.9 wt%) plates were both purchased from general market and cut into the size of 20 mm × 50 mm × 5 mm. Copper(II) sulfate pentahydrate ($CuSO_4{\cdot}5H_2O$), zinc sulfate heptahydrate ($ZnSO_4{\cdot}7H_2O$), potassium hydroxide (KOH) and ammonium persulfate ($(NH_4)_2S_2O_8$) were all analytical grade and purchased from Sinopharm Chemical Reagent Co., Ltd. Other chemical reagents including sulfuric acid (H_2SO_4, 98%), ammonia ($NH_3{\cdot}H_2O$, AR), anhydrous ethanol (AR) and acetone (AR) were purchased from West Long Chemical Co., Ltd. Pentadecafluorooctanoic acid (PFOA, 90%) with low surface energy was purchased from Aladdin.

2.2 Fabrication of superhydrophobic surfaces

As shown in Fig. 1, the single-scale nanorod structures were fabricated by electrodeposition of zinc coating and hydrothermal treatment for in situ growth of ZnO, and the dual-scale flower-like structures were fabricated by electrodeposition of copper coating and chemical oxidation for in situ growth of CuO. Then, both of them achieved superhydrophobic property after chemical modification. Before electrodeposition, the polished steel surface was first pre-treated and the detail was reported in article [29]. The specific processes of fabricating nanorod and flower-like superhydrophobic surfaces are as follows.

2.2.1 *Fabrication of ZnO nanorod structured superhydrophobic surface*

The pre-treated steel sample as cathode and the polished zinc sample as anode were immersed in the solution containing 240 g/L of $ZnSO_4{\cdot}7H_2O$ (pH ~4), and the distance between cathode and anode was 2 cm. The temperature of electrodeposition solution, the current density of direct current, and the electrodeposition time were 55 °C, 9 A/dm^2, and 26 min, respectively. Then, the steel sample was immersed in 100 mL mixed solution containing $NH_3{\cdot}H_2O$ (5 mL), anhydrous ethanol (45 mL) and distilled water (50 mL) in a Teflon-lined stainless steel reaction autoclave at 95 °C for 24 h. After the formation of ZnO nanorod structures, the steel sample was chemically modified by immersing into 0.01 mol/L of pentadecafluorooctanoic acid anhydrous ethanol solution for 11 days [30].

2.2.2 *Fabrication of CuO flower-like structured superhydrophobic surface*

The pre-treated steel sample (cathode) and the polished copper sample (anode) were put into the mixed solution composed of 200 g/L of $CuSO_4{\cdot}5H_2O$ and 12 g/L H_2SO_4 at 23 °C for 30 min with the current density of 5 A/dm^2, and the distance between cathode and anode was also maintained at 2 cm. After electrodeposition, the steel sample was immersed into the mixed solution containing 2.5 mol/L of KOH and 0.12 mol/L of $(NH_4)_2S_2O_8$ at 60 °C for 50 min. Finally, the steel sample was modified by immersing into 0.01 mol/L of pentadecafluorooctanoic acid anhydrous ethanol solution for 7 days [31].

2.3 Characterizations and tests

The surface morphologies and the crystal structures of these two superhydrophobic surfaces were observed using Field Emission Scanning Electron Microscopy (FE-SEM, Nova NanoSEM450, FEI) and X-ray diffraction (XRD, X'Pert PRO MPD, PANalytical B.V.), respectively. The contact angle was measured via the sessile liquid droplet (~5 μL) on a contact angle goniometer (SL200B, USA, KINO) in air at room temperature. The liquid droplets were gently deposited on the sample surface, and the value reported herein was the average of at least three different places on each sample.

The dynamic behaviors of a water droplet (4 μL, ~1 mm in radius) impinging on these two

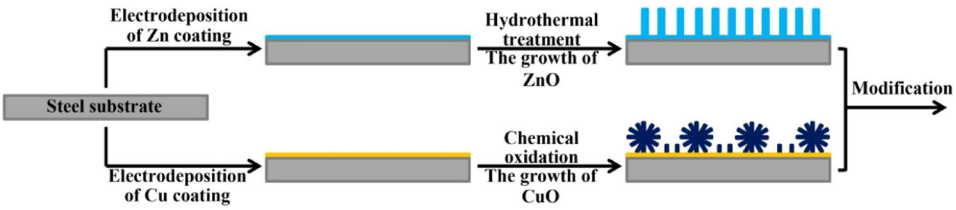

Fig. 1 Schematic illustration of fabricating single-scale ZnO nanorod and dual-scale CuO flower-like structured superhydrophobic surfaces

superhydrophobic surfaces were recorded using a high-speed camera (Photron, SA4) with 2500 fps.

The corrosion resistance of these two superhydrophobic surfaces both with an exposed area of 1 cm^2 was tested by potentiodynamic polarization in 3.5 wt% NaCl solution using electrochemical workstation (CHI 60D, China) with a standard three-electrode system at room temperature. The potentiodynamic polarization curves were obtained at a scan rate of 0.166 mV/s.

3 Results and discussion

3.1 Surface morphology and crystal structure

The surface morphologies and crystal structures of these two superhydrophobic surfaces were characterized by SEM and XRD, respectively. As shown in Fig. 2a, it can be clearly seen that nanorod structures are successfully formed on the sample surface, and the uniform nanorod structures are mostly perpendicular to the surface. Based on statistical calculations, Figure S1a shows diameter distribution histogram of the nanorod structures using the software of *Nano Measurer*, and the average diameter is about 0.15 μm. The space among the nanorod structures based on statistical calculations is showed in Figure S1b, and the average size of the space is around 0.29 μm. To confirm the crystal structure of nanorod structures, Fig. 2c shows the XRD pattern of the nanorod structured superhydrophobic surface. It can be found the diffraction peaks of wurtzite ZnO, which is consistent with article [32]. In addition, there is an obvious peak of (002), which indicates that the ZnO structures grow in orientation [33], contributing to the formation of nanorod structures.

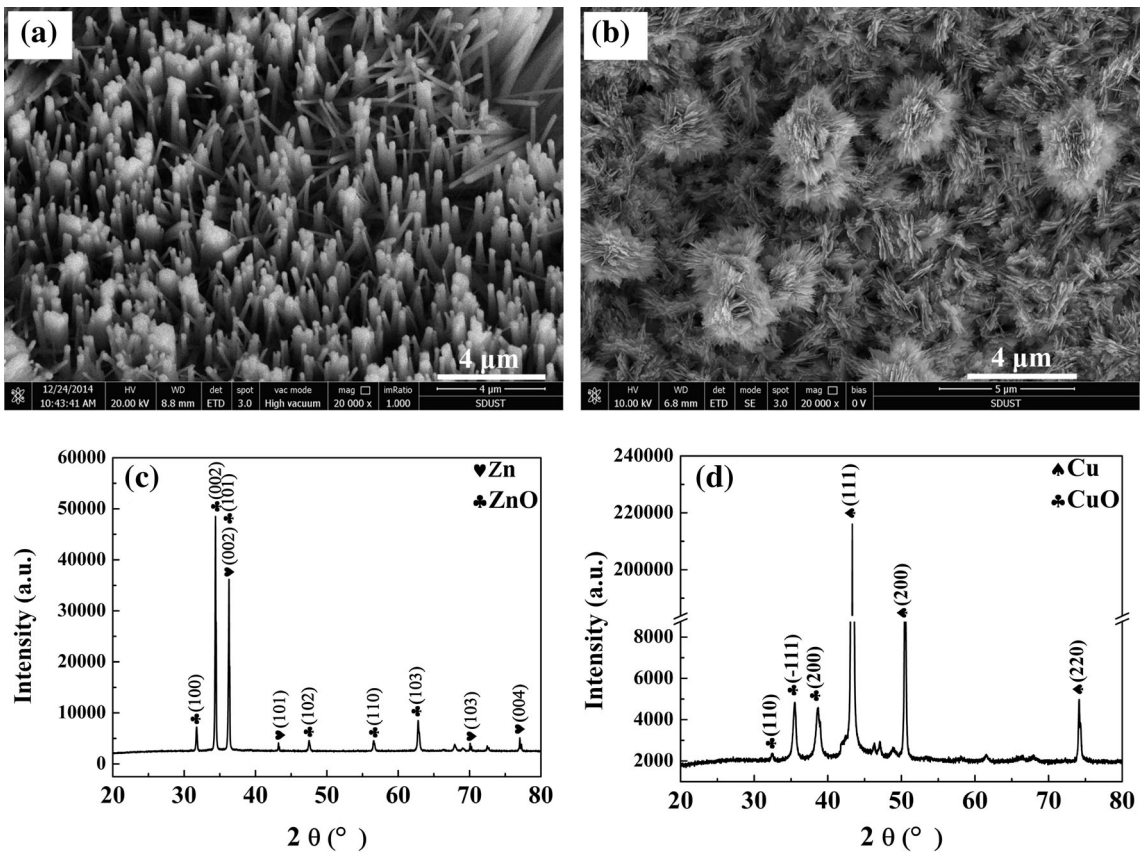

Fig. 2 SEM images (**a**, **b**) and XRD patterns (**c**, **d**) of the nanorod (**a**, **c**) and flower-like (**b**, **d**) structured superhydrophobic surfaces, respectively

As shown in Fig. 2b, it could be found that there are numerous nanosheets and some of them are clustered into flower-like structures, leading to the formation of dual-scale structure that can be seen as the composed of microsphere and nanosheet. In addition, there is certain space among the flower-like structures. Larger view of Fig. 2b is shown in Figure S2a, which is very similar to the surface microstructure of lotus leaf. As the same, the size of the nanosheet is also obtained via statistical calculations. As shown in Figure S2b, the average length of nanosheet is about 0.24 μm and the space among the nanosheet is around 0.11 μm (Figure S2c). The thickness of the nanosheet is only about 0.03 μm according to Figure S2a. The diameter of the flower-like structure is shown in Figure S2d, and the average diameter is about 2.98 μm. The space among the flower-like structures is around 2.31 μm. To confirm the crystal structure of the flower-like structure, Fig. 2d shows the XRD pattern of the flower-like structured superhydrophobic surface. It can be found that the diffraction peaks of CuO, which is consistent with article [34]. Besides, the orientation of (−111) and (200) are relatively strong, therefore, the CuO crystallites have a preferential orientation, resulting in the formation of nanosheet.

3.2 Contact angle of various liquid droplets

The wettability of the nanorod and flower-like structured superhydrophobic surfaces were analyzed by contact angles of various liquid droplets. As shown in Fig. 3, water contact angles of the nanorod and flower-like structured superhydrophobic surfaces were 157.59° and 160.69°, respectively. The sliding processes of water droplet on these two superhydrophobic surfaces are shown in Video S1 (nanorod structured surface) and Video S2 (flower-like structured surface), respectively. It can be found that the sliding angle of water droplet on the nanorod structured surface is about 6°, while that on the flower-like structured surface is only around 3°. It indicated that both the single-scale nanorod and the dual-scale flower-like structures contributed to achieving superhydrophobicity, which was consistent with Patankar's theoretical analysis [17]. In addition, glycerol contact angles on the nanorod and flower-like structured surfaces were 155.14° and 157.38°, respectively. The contact angle of 20 wt% ethanol–water (38.56 mN/m, [35]) on the nanorod and flower-like structured surfaces were 148.88° and 152.62°, respectively. The contact angle of crude oil on the nanorod structured surface was 113.85°, which was much less than that of on the flower-like structured surface (146.92°). It could be found that all of the contact angles on the nanorod structured surface were less than those of on the flower-like structured surface, indicating that the dual-scale flower-like structure was superior to the single-scale nanorod structure in realization of lyophobicity for the liquid droplet with low surface tension. This also explains the reason why most of the surface morphologies of the reported superoleophobic surface are not single-scale rough structures such as re-entrant structure [36], flower-like structure [24], or even there-level hierarchical structure [37].

As the droplets used to test the contact angles were limitation, the contact angles of the droplets with different ethanol concentrations on the nanorod and flower-like structured superhydrophobic surfaces were measured for detailed analysis of the contact angle between the droplets with different surface tension and these two superhydrophobic surfaces (the blue line in Fig. 4). Here, the ethanol–water droplets are used because water with different ethanol concentration has different surface tension [35], and the surface tension decreases with the increase of ethanol concentration (the green line in Fig. 4). It can be seen that the contact angle decreases with the increase of ethanol concentration, indicating that the contact angle decreases with decreasing the surface tension of the droplet. The contact angle on the single-scale nanorod structured surface was smaller than 150° once the ethanol concentration increased to 15 wt% (42.72 mN/m [35]), while that on the dual-scale flower-like structured surface

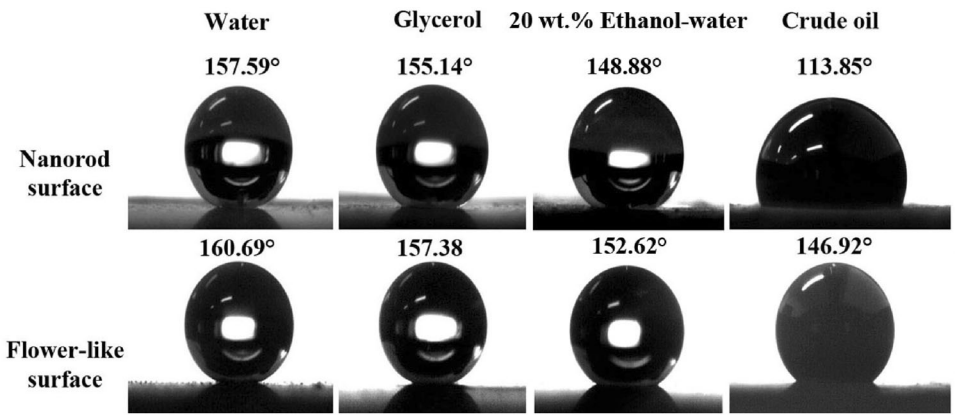

Fig. 3 Contact angles of water, glycerol, 20 wt% ethanol–water and crude oil on the nanorod and flower-like structured superhydrophobic surfaces, respectively

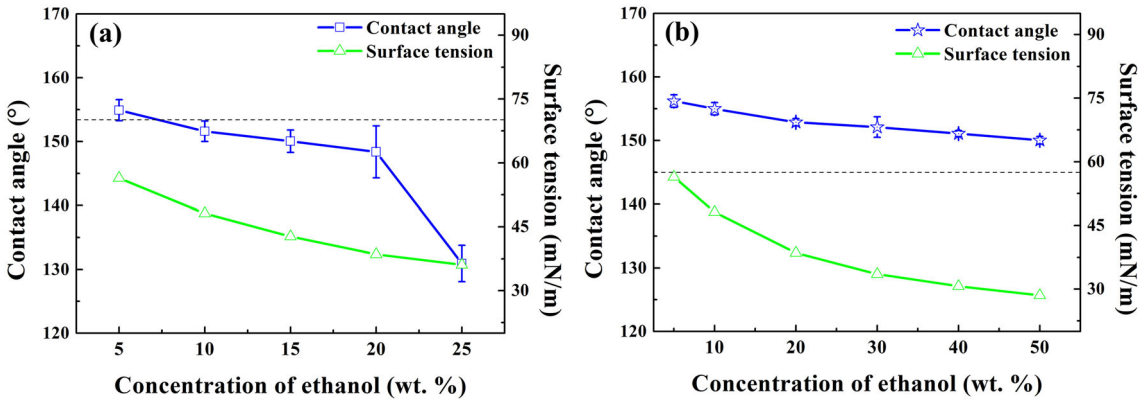

Fig. 4 Contact angles of the ethanol–water droplets on the nanorod (**a**) and flower-like (**b**) structured superhydrophobic surfaces changing with different concentration of ethanol [34]

was still larger than 150° when the ethanol concentration was 50 wt% (28.51 mN/m [35]). It further indicated that the dual-scale flower-like structure is superior to the single-scale nanorod structure in achieving the superlyophobicity.

3.3 Dynamic behavior of the impinging water droplet

In general, a water droplet is deposited gently on the sample surface in experimental works. However, water droplets contact the superhydrophobic surface often with certain velocity in practical application such as raindrop [38]. Therefore, the dynamic behavior of the impinging water droplet with different impact velocity on the nanorod and flower-like structured superhydrophobic surfaces were studied.

When the impact velocity of water droplet was small (0.31 m/s), as shown in Figure S3a, the dynamic behaviors of water droplets from contacting to complete rebounding off the nanorod and flower-like structured superhydrophobic surfaces were similar. The leaving water droplets maintained intact and did not leave any traces of adhesion on the superhydrophobic surface. With increasing the impact velocity to 0.77 m/s (Figure S3b), there were small droplets separating from the main water droplet, showing jetting phenomenon. Meanwhile, the dynamic behaviors of water droplets on these two superhydrophobic surfaces were still similar. Figure 5 shows the dynamic behaviors of the impinging water droplet with the impact velocity of 1.71 m/s. It could be found that the leaving water droplet on the flower-like structured superhydrophobic surface remained the jetting phenomenon despite the length of the main water droplet increasing (Video S3). However, the water droplet on the nanorod structured superhydrophobic surface separated many satellite droplets during the retraction process (Video S4), forming splashing phenomenon [39]. Hyungmo et al. [40] pointed out that the

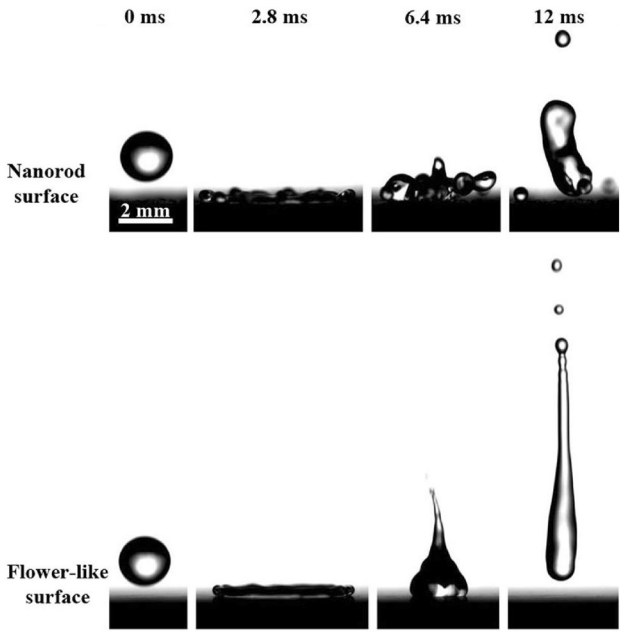

Fig. 5 Dynamic behavior of water droplet after impinging on the nanorod and flower-like structured superhydrophobic surfaces, $V = 1.71$ m/s

instability of the liquid–vapor interface could break the balance between surface tension and internal pressure of water droplet when the impact velocity was high, which could result in the formation of satellite droplets and forming splashing phenomenon. Therefore, according to these results, it could be seen that the dual-scale flower-like structured superhydrophobic surface can withstand water droplet with higher impact velocity than the single-scale nanorod structured superhydrophobic surface.

3.4 Stability and corrosion resistance

Long-term stability of the superhydrophobic surface is important in actual production. These two

superhydrophobic samples were placed in air at room temperature for 6 months, and water contact angle of these two sample surfaces was measured every month. As shown in Fig. 6a, it was found that contact angle remained stable with prolongation of the exposure time in air, showing that both the single-scale nanorod and the dual-scale flower-like structured superhydrophobic surfaces had excellent long-term stability. Thermal stability of these two superhydrophobic surfaces was measured by the method described in article [41]. The superhydrophobic samples were kept at different heating temperatures for 1 h, and the water contact angle was measured after the superhydrophobic samples cooling. The effect of heating temperature on contact angle was shown in Fig. 6b. It was found that water contact angles of these two superhydrophobic surfaces were still greater than 150° with the increase of heating temperature, showing that both the single-scale nanorod and the dual-scale flower-like structured superhydrophobic surfaces had good thermal stability.

Ultrasonic vibration is also an effective method for detecting the stability of the superhydrophobic surface [42]. Two superhydrophobic samples were placed in a beaker containing distilled water, and the beaker was placed in an ultrasonic cleaning shaker with a frequency of 45 kHz. As shown in Fig. 7a, water contact angle on the flower-like structured superhydrophobic surface maintained stable, while that on the nanorod superhydrophobic surface was decreased with the increase of ultrasonic time. This was because the flower-like structured superhydrophobic surface had dual-scale structure that can effectively prevent water into the space among microstructures, while the ability of the nanorod structures preventing water into the space was weaker, resulting in the decrease of water contact angle. Movafaghi mentioned the breakthrough pressure, which was the minimum pressure that can force a transition from the Cassie-Baxter state to the fully wetted Wenzel state [43]. The inter-nanosheet spacing of the flower-like structure is extremely small, which could lead to an extremely high breakthrough pressure. Moreover, Whyman et al. [44] mentioned that the small-scale roughness of the dual-scale structure could increase the potential barrier to be surpassed for the Cassie-Wenzel transition, thus the dual-scale flower-like structured superhydrophobic surface remained the excellent superhydrophobic property after ultrasonic vibration.

To examine corrosion resistance of these two superhydrophobic surfaces, the superhydrophobic samples were first immersed in 3.5 wt% NaCl aqueous solution at room temperature. Water contact angles of these two superhydrophobic surfaces changed with the immersion time were shown in Fig. 7b. It was found that water contact angle of the flower-like structured superhydrophobic surface was always above 150°, whereas that of the nanorod structured superhydrophobic surface was less than 150° after the immersion time increasing to 2 h. It was indicated that the dual-scale flower-like structured superhydrophobic surface had better corrosion resistance compared to the single-scale nanorod structured superhydrophobic surface.

To further evaluate the corrosion resistance of these two superhydrophobic surfaces, as shown in Fig. 8, the polarization curves of the steel substrate and these two superhydrophobic samples in 3.5 wt% NaCl aqueous solution were measured. Based on Tafel extrapolation, the corrosion potential (E_{corr}) and corrosion current density (i_{corr}) of these three samples were obtained. The E_{corr} of the single-scale nanorod structured superhydrophobic surface was −1.00493 V, which was decreased compared with the steel substrate (−0.68467 V). The i_{corr} of the nanorod structured superhydrophobic surface was 1.7117×10^{-5} A/cm^2, obvious larger than that of the steel substrate (3.9748×10^{-6} A/cm^2). It was showed that the corrosion resistance of the nanorod structured superhydrophobic surface was poor. However, the E_{corr} of the flower-like structured superhydrophobic surface (−0.21362 V)

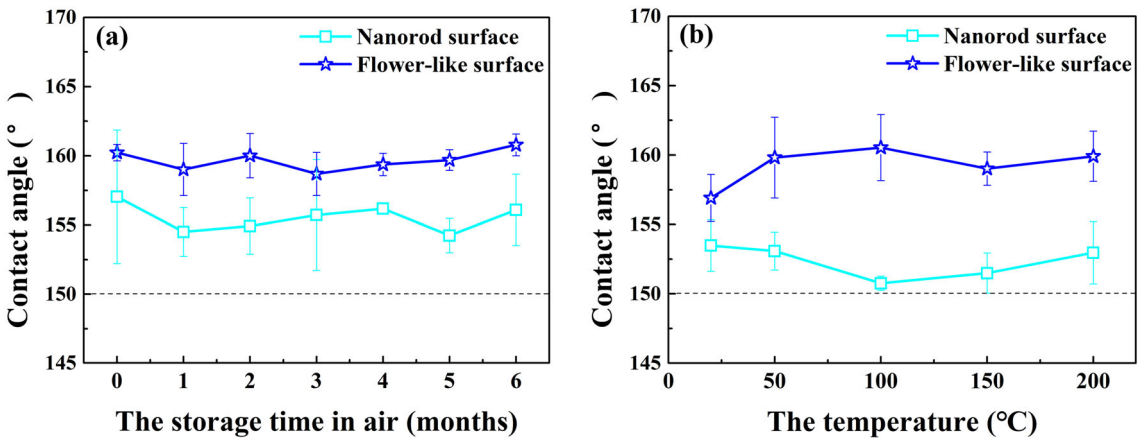

Fig. 6 Effects of the storage time in air (**a**) and the heating temperature (**b**) on water contact angle

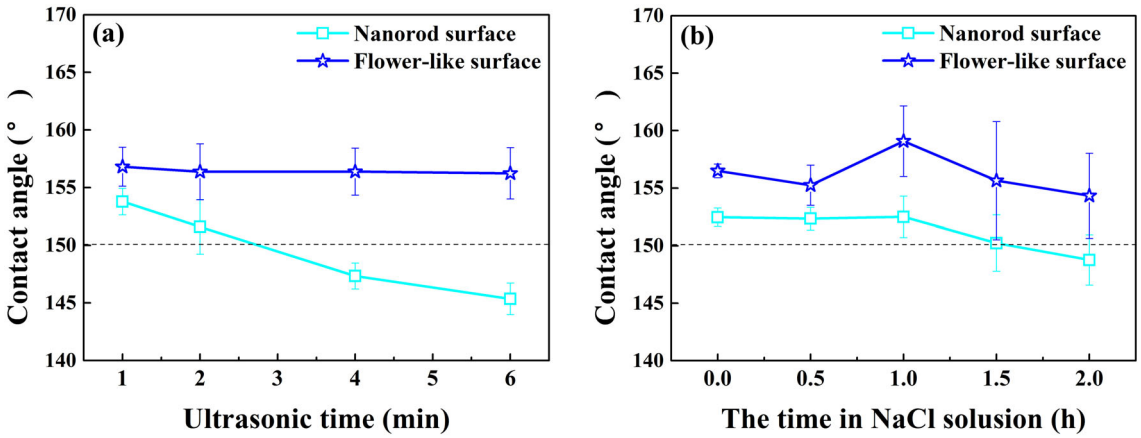

Fig. 7 Effects of the ultrasonic time (**a**) and the time immersing in NaCl solution (**b**) on water contact angle

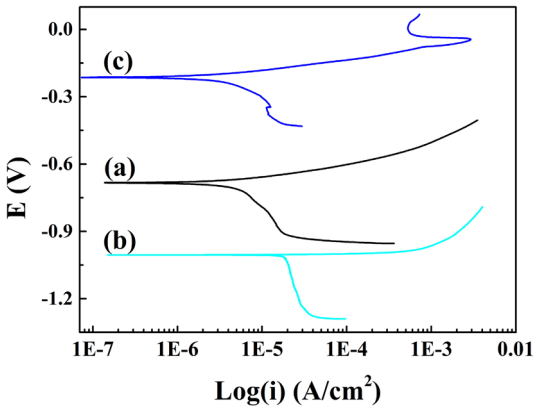

Fig. 8 Polarization curves of the pipeline steel surface (**a**), nanorod (**b**) and flower-like (**c**) structured superhydrophobic surfaces

increased and the i_{corr} (5.3899×10^{-7} A/cm^2) decreased obviously compared with those of the steel surface, showing excellent corrosion resistance.

Surface morphologies of the nanorod and flower-like structured superhydrophobic surfaces before and after corrosion were shown in Figure S4 to identify the mechanisms of corrosion resistance. It can be found that the surface morphology of the nanorod structured superhydrophobic surface before (Figure S4a) and after (Figure S4b) corrosion was basically the same and that of the flower-like structured superhydrophobic surface before (Figure S4c) and after (Figure S4d) corrosion was also unchanged. This indicated that poor corrosion resistance of the single-scale nanorod structured superhydrophobic surface was not because of the damage of surface morphology after immersing into the NaCl aqueous solution. This was mainly due to the fact that the single-scale nanorod structure on the superhydrophobic surface cannot prevent the NaCl solution trapping into the space among the microstructures, resulting in the NaCl solution contacting the zinc coating surface. Nevertheless, when the dual-scale flower-like structured superhydrophobic surface contact NaCl aqueous solution, the air trapped in the space among dual-scale structures can effectively prevent the etching solution from being immersed in the microstructure [3], and the fluoride also can be effective in preventing the diffusion of Cl^- on the superhydrophobic surface [45]. Therefore, the dual-scale flower-like structured superhydrophobic surface had excellent corrosion resistance compared with the single-scale nanorod structured superhydrophobic surface.

4 Conclusions

In conclusion, both the single-scale nanorod structure and the dual-scale flower-like structure can achieve superhydrophobicity. However, the dual-scale flower-like structure is superior to the single-scale nanorod structure in repelling the droplet with low surface tension. Meanwhile, the dual-scale flower-like structured surperhydrophobic surface had better ability for repelling the impinging water droplet with high impact velocity. Both the single-scale nanorod and the dual-scale flower-like structured surperhydrophobic surfaces had excellent long-term stability and thermal stability. Nevertheless, the dual-scale flower-like structured surface is more stable under outside vibration and had better corrosion resistance than the single-scale nanorod structured surface.

Acknowledgements The authors thank the financial support from the National Natural Science Foundation of China (51075184), the Fundamental Research Funds for the Central Universities (15CX06059A), the Postgraduate Innovative Project of China University of Petroleum (East China) (YCXJ2016036), and the project of Shengli Oil Production Plant (Shengli Oilfield Company, SINOPEC) (30200001-16-ZC0607-0035). The research group of Prof. Zuankai Wang in City University of Hong Kong helped us to obtain the dynamic videos of impinging water droplet on these two superhydrophobic surfaces.

References

1. R.X. Yuan, S.Q. Wu, P. Yu, B.H. Wang, L.W. Mu, X.G. Zhang, Y.X. Zhu, B. Wang, H.Y. Wang, J.H. Zhu, Superamphiphobic and electroactive nanocomposite toward self-cleaning, antiwear, and anticorrosion coatings. ACS Appl. Mater. Interfaces. **8**, 12481–12493 (2016)
2. L.B. Feng, M. Yang, X.T. Shi, Y.H. Liu, Y.P. Wang, X.H. Qiang, Copper-based superhydrophobic materials with long-term durability, stability, regenerability, and self-cleaning property. Colloids Surf. A **508**, 39–47 (2016)
3. L.J. Liu, W.K. Liu, R.F. Chen, X. Li, X.J. Xie, Hierarchical growth of Cu zigzag microstrips on Cu foil for superhydrophobicity and corrosion resistance. Chem. Eng. **281**, 804–812 (2015)
4. Y. Liu, J.D. Liu, S.Y. Li, J.A. Liu, Z.W. Han, L.Q. Ren, Biomimetic superhydrophobic surface of high adhesion fabricated with micronano binary structure on aluminum alloy. ACS Appl. Mater. Interfaces. **5**, 8907–8914 (2013)
5. M.K. Jung, T. Kim, H. Kim, R. Shin, J. Lee, J. Lee, J. Lee, S. Kang, Design and fabrication of a large-area superhydrophobic metal surface with anti-icing properties engineered using a top–down approach. Appl. Surf. Sci. **351**, 920–936 (2015)
6. P. Che, W. Liu, X.X. Chang, A.H. Wang, Y.S. Han, Multifunctional silver film with superhydrophobic and antibacterial properties. Nano Res. **9**, 442–450 (2016)
7. W. Barthlott, C. Neinhuis, Purity of the sacred lotus, or escape from contamination in biological surfaces. Planta **202**, 1–8 (1997)
8. D.K. Sarkar, M. Farzaneh, Fabrication of superhydrophobic surfaces on engineering materials by a solution-immersion process. Adhes. Sci. Technol. **23**, 1215 (2009)
9. B. Bhushan, Y.C. Jung, Natural and biomimetic artificial surfaces for superhydrophobicity, self-cleaning, low adhesion, and drag reduction. Prog. Mater Sci. **1**, 1–108 (2011)
10. S.Y. Li, Y. Li, J. Wang, Y.G. Nan, B.H. Ma, Z.L. Liu, J.X. Gu, Fabrication of pinecone-like structure superhydrophobic surface on titanium substrate and its self-cleaning property. Chem. Eng. **290**, 82–90 (2016)
11. M. Han, S. Go, Y. Ahn, Fabrication of superhydrophobic surface on magnesium substrate by chemical etching. B. Korean Chem. Soc. **33**, 1363–1366 (2012)
12. K. Tsujii, T. Yamamoto, T. Onda, S. Shibuichi, Super oil-repellent surfaces. Angew. Chem. Int. Ed. Eng. **9**, 1011–1012 (1997)
13. Y.S. Joung, C.R. Buie, Electrophoretic deposition of unstable colloidal suspensions for superhydrophobic surfaces. Langmuir **27**, 4156–4163 (2011)
14. Y. Shi, W. Yang, X.J. Feng, Y.S. Wang, G.R. Yue, Fabrication of superhydrophobic ZnO nanorods surface with corrosion resistance via combining thermal oxidation and surface modification. Mater. Lett. **151**, 24–27 (2015)
15. J.M. Lee, K.K. Jung, J.S. Ko, Effect of NaCl in a nickel electrodeposition on the formation of nickel nanostructure. J. Mater. Sci. **51**, 3036–3044 (2016)
16. G. Azimi, R. Dhiman, H.M. Kwon, A.T. Paxson, K.K. Varanasi, Hydrophobicity of rare-earth oxide ceramics. Nat. Mater. **12**, 315–320 (2013)
17. N.A. Patankar, Mimicking the lotus effect: influence of double roughness structures and slender pillars. Langmuir **20**, 8209–8213 (2004)
18. T.J. Li, M. Paliy, X.L. Wang, B. Kobe, W.M. Lau, J. Yang, Facile one-step photolithographic method for engineering hierarchically nano/microstructured transparent superamphiphobic surfaces. ACS Appl. Mater. Interfaces. **7**, 10988–10992 (2015)
19. H. Vahabi, W. Wang, S. Movafaghi, A.K. Kota, Free-standing, flexible, superomniphobic films. ACS Appl. Mater. Interfaces. **8**, 21962–21967 (2016)
20. S.J. Pan, A.K. Kota, J.M. Mabry, A. Tuteja, Superomniphobic surfaces for effective chemical shielding. J. Am. Chem. Soc. **135**, 578–581 (2013)
21. H. Kim, K. Noh, C. Choi, J. Khamwannah, D. Villwock, S. Jin, Extreme superomniphobicity of multiwalled 8 nm TiO_2 nanotubes. Langmuir **27**, 10191–10196 (2011)
22. Y. Liu, H.J. Cao, S.G. Chen, D.A. Wang, Ag nanoparticle-loaded hierarchical superamphiphobic surface on an al substrate with enhanced anticorrosion and antibacterial properties. J. Phys. Chem. C **119**, 25449–25456 (2015)
23. H. Jin, M. Kettunen, A. Laiho, H. Pynnonen, J. Paltakari, A. Marmur, O. Ikkala, R.H.A. Ras, Superhydrophobic and superoleophobic nanocellulose aerogel membranes as bioinspired cargo carriers on water and oil. Langmuir **27**, 1930–1934 (2011)
24. L.W. Chen, Z.G. Guo, W.M. Liu, biomimetic multi-functional superamphiphobic FOTS-TiO_2 particles beyond lotus leaf. ACS Appl. Mater. Interfaces. **8**, 27188–27198 (2016)
25. W.J. Jiang, C.M. Grozea, Z.Q. Shi, G.J. Liu, Fluorinated raspberry-like polymer particles for superamphiphobic coatings. ACS Appl. Mater. Interfaces. **6**, 2629–2638 (2014)
26. S.Y. Lee, Y. Rahmawan, S. Yang, Transparent and superamphiphobic surfaces from mushroom-like micropillar arrays. ACS Appl. Mater. Interfaces. **7**, 24197–24203 (2015)
27. H.J. Li, X.B. Wang, Y.L. Song, Y.Q. Liu, Q.S. Li, L. Jiang, D.B. Zhu, Super-amphiphobic aligned carbon nanotube films. Angew. Chem. Int. Ed. **40**, 1743–1745 (2001)
28. A. Tutejaa, W. Choib, J.M. Mabryc, G.H. McKinleyb, R.E. Cohena, Robust omniphobic surfaces. PNAS **105**, 18200–18205 (2008)
29. H. Li, S.R. Yu, X.X. Han, Preparation of a biomimetic superhydrophobic ZnO coating on an X90 pipeline steel surface. New J. Chem. **39**, 4860–4868 (2015)
30. H. Li, S.R. Yu, Facile fabrication of micro–nano-rod structures for inducing a superamphiphobic property on steel surface. Appl. Phys. A **122**, 30 (2016)
31. H. Li, S.R. Yu, X.X. Han, Fabrication of CuO hierarchical flower-like structures with biomimetic superamphiphobic, self-cleaning and corrosion resistance properties. Chem. Eng. **283**, 1443–1454 (2016)
32. B. Liu, H.C. Zeng, Hydrothermal synthesis of ZnO nanorods in the diameter regime of 50 nm. J. Am. Chem. Soc. **125**, 4430–4431 (2003)
33. A. Gomes, T. Frade, Isabel D. Nogueira, Morphological characterization of Zn-based nanostructured thin films. Curr. Microsc. Contrib. Adv. Sci. Technol. **2**, 1146–1153 (2012)
34. D.Q. Gao, G.J. Yang, J.Y. Li, J. Zhang, J.L. Zhang, D.S. Xue, Room-temperature ferromagnetism of flowerlike CuO nanostructures. J. Phys. Chem. C **114**, 18347–18351 (2010)
35. G. Vazquez, E. Alvarez, J.M. Navaza, Surface tension of alcohol water + water from 20 to 50 °C. J. Chem. Eng. Data **40**, 611–614 (1995)
36. W.S.Y. Wong, G.Y. Liu, N. Nasiri, C.L. Hao, Z.K. Wang, Antonio tricoli, omnidirectional self-assembly of transparent superoleophobic nanotextures. ACS Nano **11**, 587–596 (2017)
37. A.R. Bielinski, M. Boban, Y. He, E. Kazyak, D.H. Lee, C.M. Wang, A. Tuteja, N.P. Dasgupta, Rational design of hyperbranched nanowire systems for tunable superomniphobic surfaces enabled by atomic layer deposition. ACS Nano **11**, 478–489 (2017)
38. Y.Z. Shen, J. Tao, H.J. Tao, S.L. Chen, L. Pan, T. Wang, Relationship between wetting hysteresis and contact time of a bouncing droplet on hydrophobic surfaces. ACS Appl. Mater. Interfaces. **7**, 20972–20978 (2015)
39. P. Tsai, S. Pacheco, C. Pirat, L. Lefferts, D. Lohse, Drop impact upon micro- and nanostructured superhydrophobic surfaces. Langmuir **25**, 12293–12298 (2009)

40. H. Kim, C. Lee, M.H. Kim, J. Kim, Drop impact characteristics and structure effects of hydrophobic surfaces with micro- and/or nanoscaled structures. Langmuir **28**, 11250–11257 (2012)
41. K. Seo, M. Kim, S. Seok, D.H. Kim, Transparent superhydrophobic surface by silicone oil combustion. Colloids Surf. A **492**, 110–118 (2016)
42. Z. Chen, X.J. Liu, Y. Wang, J. Li, Z.S. Guan, Highly transparent, stable, and superhydrophobic coatings based on gradient structure design and fast regeneration from physical damage. Appl. Surf. Sci. **359**, 826–833 (2015)
43. S. Movafaghi, V. Leszczak, W. Wang, J.A. Sorkin, L.P. Dasi, K.C. Popat, A.K. Kota, Hemocompatibility of superhemophobic titania surfaces. Adv. Healthc. Mater. **6**, 1600717 (2017)
44. G. Whyman, E. Bormashenko, How to make the Cassie wetting state stable? Langmuir **27**, 8171–8176 (2011)
45. H.F. Zhang, L. Yin, S.Y. Shi, X.W. Liu, Y. Wang, F. Wang, Facile and fast fabrication method for mechanically robust superhydrophobic surface on aluminum foil. Microelectron. Eng. **141**, 238–242 (2015)